

ZigZag: Universal Sampling-free Uncertainty Estimation Through Two-Step Inference

Nikita Durasov¹ Nik Dorndorf² Pascal Fua¹

¹Computer Vision Laboratory, EPFL, {name.surname}@epfl.ch

²RWTH Aachen, {name.surname}@rwth-aachen.de

Abstract

Whereas the ability of deep networks to produce useful predictions on many kinds of data has been amply demonstrated, estimating the reliability of these predictions remains challenging. Sampling approaches such as MC-Dropout and Deep Ensembles have emerged as the most popular ones for this purpose. Unfortunately, they require many forward passes at inference time, which slows them down. Sampling-free approaches can be faster but suffer from other drawbacks, such as lower reliability of uncertainty estimates, difficulty of use, and limited applicability to different types of tasks and data.

In this work, we introduce a sampling-free approach that is generic and easy to deploy, while producing reliable uncertainty estimates on par with state-of-the-art methods at a significantly lower computational cost. It is predicated on training the network to produce the same output with and without additional information about that output. At inference time, when no prior information is given, we use the network’s own prediction as the additional information. We prove that the difference between the two predictions is an accurate uncertainty estimate and demonstrate our approach on various types of tasks and applications.

1. Introduction

Though the ability of modern neural networks to generate accurate predictions is now clear, assessing the trustworthiness of these predictions remains an open problem.

Among all the uncertainty estimation methods, MC-Dropout [16] and Deep Ensembles [25] are the most widely used. MC-Dropout involves randomly zeroing out network weights and assessing the effect, whereas Ensembles involve training multiple networks, starting from different initial conditions. They are simple to deploy and universal. Unfortunately, they induce substantial computational and memory overheads, which makes them unsuitable for many real-world applications.

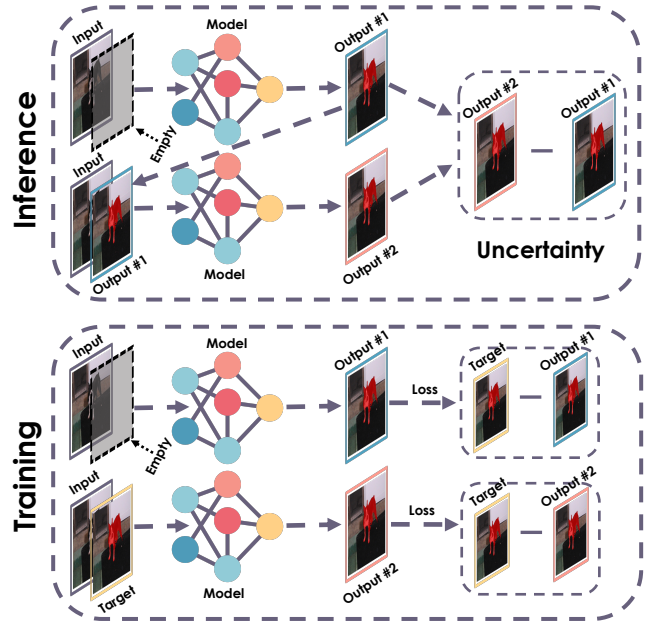


Figure 1. **ZigZag Architecture.** Given a single RGB image x and corresponding target y , our model can make predictions in two different ways, either using just information about x with $[x, 0]$ as input or using both input x and target y with $[x, y]$ as input. This modification regularizes the model and, crucially, enables uncertainty estimation. At inference time, we make two forward passes. First, we use $[x, 0]$ as input to produce initial prediction y_1 . Second, we feed $[x, y_1]$ to the network and generate y_2 . The difference between y_1 and y_2 serves as our uncertainty estimate.

An alternative is to use sampling-free methods that estimate uncertainty in one single forward pass of a single neural network, thereby avoiding computational overheads [1, 31, 36, 43]. However, deploying them usually requires heavily modifying the network’s architecture [36], significantly changing the training procedures [31], or limiting oneself to very specific tasks [1, 31, 34]. As a result, they have not gained as much traction as MC-Dropout and Ensembles.

To remedy this, we introduce *ZigZag*, a sampling-free approach that is generic and easy to deploy, while producing

reliable uncertainty estimates on par with sampling-based methods at a significantly lower computational cost. It is predicated on the following insight: Given a sample \mathbf{x} for which a generic network \mathcal{M} has learned to accurately predict target $\mathbf{y} = \mathcal{M}(\mathbf{x})$, providing information about the desired value of \mathbf{y} during the forward pass should not change the inference. By contrast, if the prediction is inaccurate, providing such information should help significantly. To leverage this insight, we slightly modify the first layer of \mathcal{M} so that it can accept a second argument, as shown in Fig. 1 (Training). We then train it so that, for all training pairs (\mathbf{x}, \mathbf{y}) in a training set, we have $\mathbf{y} \approx \mathcal{M}(\mathbf{x}, \mathbf{0}) \approx \mathcal{M}(\mathbf{x}, \mathbf{y})$, where $\mathbf{0}$ is a vector of zeros. At inference time, we run the forward pass twice as shown in Fig. 1 (Inference): We first compute $\mathcal{M}(\mathbf{x}, \mathbf{0})$ and then $\mathcal{M}(\mathbf{x}, \mathcal{M}(\mathbf{x}, \mathbf{0}))$. In other words, since we do not have prior information about the answer, we use the prediction of the network as a proxy for it. We show that the difference between these two predictions is a good predictor of the networks uncertainty. More formally, we prove that if the network exhibits Lipschitz regularity properties, which most networks do [42, 45], $\|\mathcal{M}(\mathbf{x}, \mathbf{0}) - \mathcal{M}(\mathbf{x}, \mathcal{M}(\mathbf{x}, \mathbf{0}))\|$ can be used to bound the prediction error.

Our approach is fast because it only requires performing two forwards passes using one single network and delivers uncertainty results comparable to those of Ensembles, which are much more costly but often seen as the method that delivers the best uncertainty estimates on a wide range of problems. Furthermore, it is very easy to use in conjunction with almost any network architecture with only very minor changes. Hence, our method is also task-agnostic.

2. Related work

Uncertainty Estimation (UE) aims to accurately evaluate the reliability of a model’s predictions. Among all the methods that can be used to do this, MC-Dropout [16] and Deep Ensembles [25] have emerged as two of the most popular ones, with Bayesian Networks [29] being a third alternative. These methods are sampling-based and require several predictions at inference time, which slows them down. Hence, there has been recent work in trying to overcome this drawback. We discuss both kinds of approaches below.

Sampling-based Approaches. MC-Dropout involves randomly zeroing out network weights and assessing the effect, whereas Ensembles involve training multiple networks, starting from different initial conditions. The extensive survey of [2] concludes that Deep Ensembles tend to produce the most decorrelated models, which results in highly diversified predictions and the most reliable uncertainty estimates. Unfortunately, Deep Ensembles also entail the highest computation costs due to the need to train multiple networks and to run up to dozens of

forward passes at inference time. MC-Dropout tends to be less reliable and also involves making several inferences at inference time. There have been recent attempts at increasing the reliability of MC-Dropout [12, 47] but they do not address the fact that multiple inferences are required to estimate the uncertainty. Bayesian Networks also require several forward passes to compute uncertainty and rarely outperform Deep Ensembles.

Sampling-free Approaches. When a rapid response is needed, for example for robotic control [28] or low-latency [15] applications, there is no time to perform many forward passes during inference. Consequently, there has been much recent interest for sampling-free approaches that do not require it. For example, in [1], a clustering-like procedure is used to estimate uncertainty for classification and semantic segmentation purposes. In [30, 31], uncertainty is estimated from Dirichlet and Normal-Wishart distributions whose parameters are predicted by the network.

Unfortunately, there rarely is a clear way to extend these mostly classification approaches to handle regression. Furthermore, deploying them requires significantly changing both the original networks architecture and the training procedures, which limits their appeal.

Regression is handled in [36] using an uncertainty estimation method that relies on uncertainty propagation from one layer to another. During the forward pass, not only activations but also their variances are estimated in each layer. Thus, the variance of the final predictions can be estimated in one pass but at the cost of a two-fold memory consumption. In [43], both quantile regression [14] and *orthonormal certificates* are used to detect out-of-distribution samples during inference. Though being computationally efficient, this approach also can result in poor uncertainty estimates and miscalibrated predictions. Recent SNGP [27] approach is also used to estimate uncertainty in a deep learning context, but this requires adding a Random Features [38] and Spectral Normalization [32] layer to every convolutional layer, which entails significant modifications of both training dynamic and network architectures. Furthermore, in some cases, they can yield significantly worse uncertainty calibration than sampling-based approaches [37]. We provide our own comparisons in the experiment section.

3. Method

ZigZag is an approach to sampling-free uncertainty estimation that delivers classification and regression results on par with state-of-the-art sampling-based methods such as Ensembles and MC-Dropout while being far less computationally demanding. In this section, we develop the central idea that underlies *ZigZag*, offer theoretical justifications for it, and provide implementation details.

3.1. ZigZag Approach

We start from the following intuition: Given a sample \mathbf{x} for which a deep network \mathcal{M} has already learned to accurately predict target \mathbf{y} , providing information about \mathbf{y} during the forward pass would not change the inference. By contrast, if the prediction is inaccurate providing such information will have a significant impact, which is a red flag.

To implement this idea, let us assume that \mathcal{M} takes as input a vector \mathbf{x} and returns a prediction vector $\mathbf{y} = \mathcal{M}(\mathbf{x})$. In practice, \mathcal{M} can be any sufficiently powerful deep architecture, such as VGG [41], ResNet [18] or Transformers [10], with one minor change. If the original architecture takes as input a vector \mathbf{x} , the modified one should take as input both \mathbf{x} and a vector of the same dimension as \mathbf{y} so that we can compute $\mathcal{M}(\mathbf{x}, \mathbf{y}_e)$, where \mathbf{y}_e is a vector of the same dimension as \mathbf{y} . At training time, when ground-truth data is available, we train \mathcal{M} to return similar results whether \mathbf{y}_e is the ground-truth value or if $\mathbf{y}_e = \mathbf{0}$, a vector of zeros. In other words, providing prior information about the target should have little impact. At inference time, ground-truth values are no longer available and we replace them by the networks own estimate. Meaning, we compute both $\mathcal{M}(\mathbf{x}, \mathbf{0})$ and $\mathcal{M}(\mathbf{x}, \mathcal{M}(\mathbf{x}, \mathbf{0}))$. We show below that the distance between these two predictions is a good uncertainty estimate. The training and inference modes are depicted by Fig. 1.

3.2. Theoretical Justification

As discussed above, at inference time, given a sample \mathbf{x} , we compute

$$\begin{aligned} \mathbf{y}_0 &= \mathcal{M}(\mathbf{x}, \mathbf{0}) , \\ \mathbf{y}_1 &= \mathcal{M}(\mathbf{x}, \mathbf{y}_0) = \mathcal{M}(\mathbf{x}, \mathcal{M}(\mathbf{x}, \mathbf{0})) \end{aligned} \quad (1)$$

Assuming that \mathcal{M} has been properly trained, \mathbf{y}_0 and \mathbf{y}_1 should be similar and close to the target value. We therefore write

$$\begin{aligned} \hat{\mathbf{y}} &= \mathcal{M}(\mathbf{x}, \mathbf{0}) = \mathbf{y}_0 , \\ \hat{\mathbf{u}} &= \|\mathbf{y}_0 - \mathbf{y}_1\| , \end{aligned} \quad (2)$$

where $\hat{\mathbf{y}}$ is the final network prediction and $\hat{\mathbf{u}}$ is taken to be the corresponding uncertainty estimate. In other words, we use the distances between the predictions \mathbf{y}_0 and \mathbf{y}_1 as a proxy for uncertainty, which we now justify.

The standard triangular inequality allows us to write

$$\begin{aligned} \|\mathbf{y}_1 - \mathbf{y}_0\| &\leq \|\mathbf{y}_1 - \mathbf{y}\| + \|\mathbf{y} - \mathbf{y}_0\| , \\ \|\mathbf{y} - \mathbf{y}_0\| &\leq \|\mathbf{y}_1 - \mathbf{y}\| + \|\mathbf{y}_1 - \mathbf{y}_0\| , \end{aligned} \quad (3)$$

where \mathbf{y} is the *true* value we seek to estimate.

Furthermore, most practical network architectures satisfy Lipschitz inequality constraints [42,45]. Hence, we can

safely assume that \mathcal{M} is Lipschitz, meaning that

$$\begin{aligned} \exists L_{\mathcal{M}}^d \in \mathbb{R}_{>0}, \forall \mathbf{z}_1, \mathbf{z}_2 \in \mathbb{R}^M, \\ \|\mathcal{M}(\mathbf{z}_1) - \mathcal{M}(\mathbf{z}_2)\| \leq L_{\mathcal{M}}^d \|\mathbf{z}_1 - \mathbf{z}_2\| . \end{aligned} \quad (4)$$

This is because many of the standard network layers—Linear, Conv, ReLU, BatchNorm, Downsampling—are Lipschitz. Hence, $L_{\mathcal{M}}^d$, the Lipschitz constant of the whole model, is the product of the Lipschitz constants of its individual layers. Thus, $L_{\mathcal{M}}^d$ can be large but always finite. In Section 4.5, we show empirically that $L_{\mathcal{M}}^d$ does not have to be large for practical tasks. Let us further assume that

$$\begin{aligned} \exists L_{\mathcal{M}}^u \in \mathbb{R}_{>0}, \forall \mathbf{z}_1, \mathbf{z}_2 \in \mathbb{R}^M / \{\mathbf{0}\}, \\ \|(\mathbf{x}, \mathbf{z}_1) - (\mathbf{x}, \mathbf{z}_2)\| = \|\mathbf{z}_1 - \mathbf{z}_2\| \leq \\ \leq L_{\mathcal{M}}^u \|\mathcal{M}(\mathbf{x}, \mathbf{z}_1) - \mathcal{M}(\mathbf{x}, \mathbf{z}_2)\| \end{aligned} \quad (5)$$

for $L_{\mathcal{M}}^u < 1$, which means that given different optional inputs \mathbf{z}_1 and \mathbf{z}_2 our model generates different predictions. This is a weak form of being bi-Lipschitz and a reasonable assumption because many networks, such as ResNets [18], can be trained to be bi-Lipschitz. We prove in the supplementary material that injecting Eqs. 3, 4, and 5 into Eq. 2 yields

$$\frac{1}{1 + L_{\mathcal{M}}^d} \|\mathbf{y}_0 - \mathbf{y}_1\| \leq \|\mathbf{y}_0 - \mathbf{y}\| \leq \frac{L_{\mathcal{M}}^u}{1 - L_{\mathcal{M}}^u} \|\mathbf{y}_0 - \mathbf{y}_1\| . \quad (6)$$

Note that proving the left part of the inequality requires the existence of $L_{\mathcal{M}}^d$ but not that of $L_{\mathcal{M}}^u$. Conversely, proving the other side of the equality requires the existence of $L_{\mathcal{M}}^u$ and it being smaller than 1. In other words, if the network satisfies the condition from Eq. 5, we get better theoretical guarantees and tighter error bounds than if it is simply Lipschitz. These are practical requirements because there are ways to ensure that this condition is met [3]. For the sake of simplicity and practicality, we do not do this explicitly. Nevertheless, as shown in Section 4.5, we get meaningful error bounds. In any event, the left side of Eq. 6 that always holds motivates using $\|\mathbf{y}_0 - \mathbf{y}_1\|$ as an uncertainty measure. Our experiments confirm the validity of this choice.

3.3. Modifying the Architecture

Given a standard architecture \mathcal{M} that takes one input \mathbf{x} , we have to modify it so that it accepts two.

For clarity, let us first consider the case where \mathcal{M} is a simple network with one hidden layer of dimension h , as shown in Fig. 2. It takes $\mathbf{x} \in \mathbb{R}^d$ as input and outputs a scalar $y \in \mathbb{R}$. To handle a second argument y_e , the input dimension of the first trainable layer must become $d + 1$ to allow the concatenation of the original input vector \mathbf{x} and the additional value y_e .

Similarly we can add additional channels to convolutional layers to work with RGB images, for example by

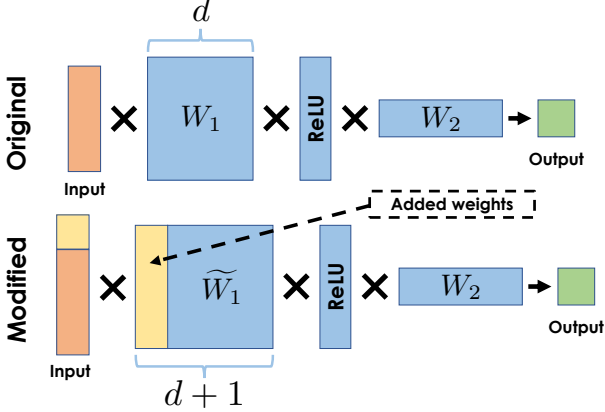


Figure 2. **Architecture Modification.** Given a model with weights $W_1 \in \mathbb{R}^{d \times h}$, $W_2 \in \mathbb{R}^{h \times 1}$, we modify its first layer W_1 to accept two inputs instead of only one. The modified model consists of $\tilde{W}_1 \in \mathbb{R}^{(d+1) \times h}$ and $W_2 \in \mathbb{R}^{h \times 1}$ and can process the concatenation of the original input \mathbf{x} and additional value \mathbf{y}_0 .

adding a fourth channel that represents y_e . As before, we only need to modify the first convolutional layer of the network so that it can process 4-dimensional inputs.

3.4. Training

At the heart of our approach is training \mathcal{M} to produce similar results whether or not a *target* \mathbf{y} is provided as input. Hence, given a training sample (\mathbf{x}, \mathbf{y}) , we randomly decide with probability p whether to provide \mathbf{y} as an input or not. We then take the loss to be

$$\mathcal{L}(\mathcal{M}(\mathbf{x}), \mathbf{y}) = \begin{cases} \mathcal{L}_{dat}(\mathcal{M}(\mathbf{x}, \mathbf{0}), \mathbf{y}) & \text{if } \zeta \geq p \\ \mathcal{L}_{dat}(\mathcal{M}(\mathbf{x}, \mathbf{y}), \mathbf{y}) & \text{otherwise} \end{cases} \quad (7)$$

where $\zeta \sim \text{Uniform}(0, 1)$ and \mathcal{L}_{dat} is a domain dependent loss term whose minimization ensures that the prediction of \mathcal{M} is close to the target. Setting $p = 0.0$ would yield to original model training. In our experiments, we set $p = 0.5$ to give equal importance of both regimes. Minimizing this loss ensures that

$$\mathcal{M}(\mathbf{x}, \mathbf{0}) \approx \mathcal{M}(\mathbf{x}, \mathbf{y}) \approx \mathbf{y}, \quad (8)$$

which is what was mentioned in Section 3.1 and is required for the proof in the supplementary material.

4. Experiments

We first introduce our metrics and baselines. We then use simple synthetic data to illustrate the behavior of *ZigZag*. Next, we turn to image datasets often used to test uncertainty-estimation algorithms. Finally, we present real-world applications.

4.1. Metrics and Baselines

In this section, we introduce the evaluation metrics which we use to quantitatively compare our methods against

several baselines. Additional details are provided in supplementary material.

Accuracy Metric. For classification tasks, we use the standard classification accuracy, i.e. the percentage of correctly classified samples on the test set. For regression tasks, we use the standard *Mean Absolute Error* (MAE) metric.

Uncertainty Metrics. As in [37], we use *Relative Area Under the Lift Curve* (rAULC) to quantify the quality of calibration of uncertainty measures both for classification and regression tasks. Unlike other metrics [5, 17], it is suitable for sampling-free approaches to estimate uncertainty.

Another way to estimate how good uncertainty estimates are is to use them to detect out-of-distribution samples under the assumption that the network is more uncertain about those than about samples from the distribution used to train it. As in [12, 31], given both in- and out-of-distribution (OOD) samples, we classify high-uncertainty ones as OOD and rely on standard classification metrics, ROC and PR AUCs, to quantify the classification performance.

Time, Memory, and Simplicity. The *Time* and *Size* metrics measure how much time and memory it takes to train the network(s) to estimate uncertainty, compared to a single one that does not estimate it. The *Simplicity* metric assesses how easy it is to modify a given architecture to obtain uncertainty estimates. We denote it as simple (✓) if it requires changing less than 10% of layers of the original model and the training procedures does not need to be substantially modified. We also report *Inference Time* that represents how much time the model takes to compute uncertainties relative to single model inference without them.

Baselines. We compare against recent sample-based approaches—MC-Dropout [16] (*MC-D*), Deep Ensembles [25] (*DeepE*), BatchEnsemble [48] (*BatchE*) and Masksembles [12] (*MaskE*)—and sample-free ones—Single Model [22] (*Single*), Orthonormal Certificates [44] (*OC*), SNGP [27] (*SNGP*), Variance Propagation [36] (*VarProp*). For all four sampling-based approaches, we use five samples to estimate the uncertainty at inference time. This number of samples has been shown to perform well for many tasks [12, 31, 48]. All of the training and implementation details are provided in supplementary material.

4.2. Simple Synthetic Data.

We use such data to illustrate how *ZigZag* behaves both for classification and regression.

Classification Task. Let us consider the red and blue 2D points shown in Fig. 3. We use them to train an MLP with 6 fully-connected layers and LeakyReLU activations to classify other points in the plane as belonging either to the red or the blue class. The background color in each of the

subplots depicts the uncertainty estimated by Single-Model, MC-Dropout, Deep Ensembles, and *ZigZag*. The first two only exhibit uncertainty along a narrow band between the two distributions. This is highly questionable once one is far away from the data points in the lower left and upper right corners of the range. Both Ensembles and *ZigZag* deliver more plausible high uncertainties once far from the training points, but *ZigZag* does it at a lower computational cost.

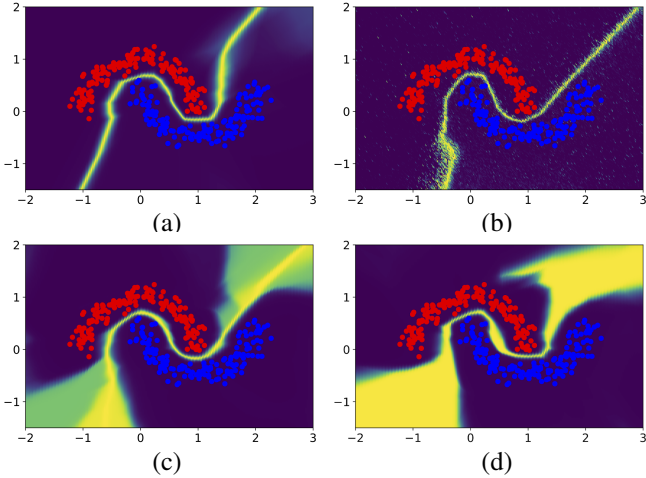


Figure 3. **Uncertainty Estimation for Classification.** The task is to classify data points drawn in the range $x \in [-2, 3]$, $y \in [-2, 2]$ as being red or blue given the red and blue training samples from two interleaving half circles with added Gaussian noise. The background color depicts the classification uncertainty assigned by different techniques to individual grid points. Violet is low and yellow is high. (a) Single model, (b) MC-Dropout, (c) Deep Ensembles, (d) *ZigZag*.

Regression Task. Let us now consider the simple regression problem depicted by Fig. 4: We draw values x in the range $[-1, 3]$, compute values $y = f(x) + \sigma$ where f is the third order polynomial and σ is Gaussian noise, and use these pairs to train a regression network. The shaded areas depict the uncertainty estimated by Single-Model, MC-Dropout, Deep Ensembles, and *ZigZag*. For the points outside of the training range, the last two correctly predict very large uncertainties, unlike the first two. But again, *ZigZag* does it at a lower computational cost than Deep Ensembles.

4.3. Classification Tasks.

We now compare *ZigZag* against the baselines on the widely used benchmark datasets depicted by Fig. 5. The images are very different across datasets and exhibit distinct statistics. We performed two distinct experiments that we describe in more detail below.

We report the results in Tab 1. In both cases, Deep Ensembles and *ZigZag* perform similarly and outperform the other approaches. However, *ZigZag* does not incur the 5-fold increase in memory and time requirements that Deep

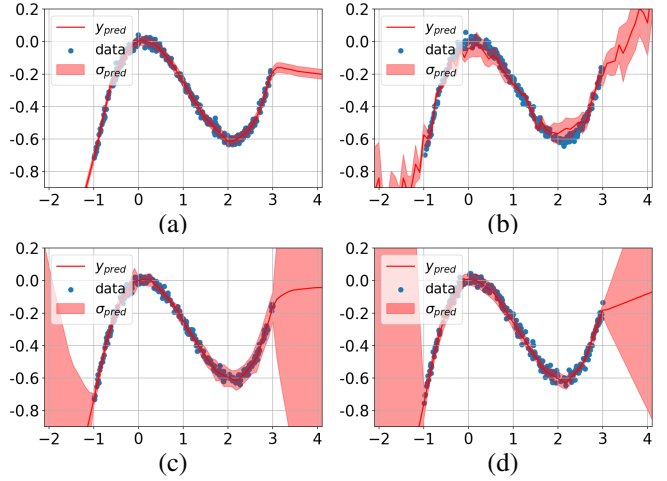


Figure 4. **Uncertainty Estimation for Regression.** The task is to regress y -axis values for x -axis data points drawn in the range $x \in [-1, 3]$ from third power polynomial with added Gaussian noise. Red colored area depicts the uncertainty assigned by different models to individual points on the x -axis grid. (a) Single model, (b) MC-Dropout, (c) Deep Ensembles, (d) *ZigZag*.

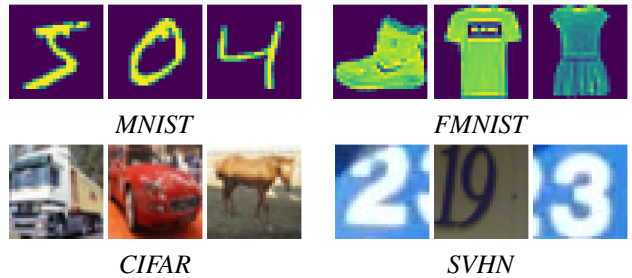


Figure 5. **Classification datasets.** (MNIST vs FashionMNIST) Both datasets feature ten classes—10 digits for one and 10 types of clothes for the other—depicted by 8-bit of 28×28 images. (CIFAR vs SVHN) Both datasets feature ten classes—ten animals and vehicles for one and 10 road sign digits for the other—depicted by 32×32 RGB images.

Ensembles does. Note that sampling-free approaches tend to yields worse calibration than sampling-based ones [37]. Our model is not impacted by this.

MNIST vs FashionMNIST. We train networks on MNIST [26] and compute the accuracy and calibration metrics. We then use the uncertainty measure they produce to classify images from the test sets of MNIST and FashionMNIST [49] as being within the MNIST distribution or not to compute the OOD metrics introduced in Section 4.1. We use a standard architecture with four convolution and pooling layers, followed by fully connected layers with ReLU activations.

CIFAR vs SVHN. We ran a similar experiment with the CIFAR10 [24] and SVHN [35] datasets. This is challenging for OOD detection because many of the CIFAR 32×32 images are noisy and therefore hardly distinguishable from each other, which makes the class labels unreliable. As the training set is relatively small, very large models tend to

	MC-D	DeepE	BatchE	MaskE	Single	OC	SNGP	VarProp	ZigZag	
Accuracy	0.981	0.990	0.989	0.989	0.980	0.980	0.984	0.986	0.982	MNIST
rAUC	0.932	0.958	0.941	0.929	0.712	0.851	0.813	0.731	0.961	
Size	1x	5x	1.2x	1x	1x	1.3x	1x	1x	1x	
Inf. Time	5x	5x	5x	5x	1x	1.4x	1.7x	1.2x	2x	
Time	1.3x	5x	1.4x	1.3x	1x	1.1x	1.1x	1.x	1x	
ROC-AUC	0.953	0.984	0.965	0.963	0.773	0.934	0.951	0.812	0.982	
PR-AUC	0.962	0.979	0.965	0.966	0.844	0.923	0.942	0.861	0.981	
Accuracy	0.909	0.929	0.911	0.901	0.8901	0.892	0.905	0.895	0.928	CIFAR
rAUC	0.889	0.911	0.884	0.889	0.884	0.583	0.742	0.715	0.897	
Size	1x	5x	1.2x	1x	1x	1x	1x	1x	1x	
Inf. Time	5x	5x	5x	5x	1x	1.1x	1.1x	1.2x	2x	
Time	1.2x	5x	1.4x	1.3x	1x	1.3x	1x	1.2x	1.2x	
ROC-AUC	0.854	0.915	0.877	0.900	0.825	0.851	0.900	0.831	0.901	
PR-AUC	0.918	0.949	0.919	0.931	0.8747	0.821	0.891	0.861	0.933	
Simple	✓	✓	✗	✗	-	✓	✗	✗	✓	

Table 1. **Classification results on MNIST (top) and CIFAR (bottom).** The best result in each category is in **bold** and the second best is in **bold**. Most correspond to *ZigZag* and *DeepE*. Hence, they perform similarly but *ZigZag* requires far less computation and memory.

	MC-D	DeepE	BatchE	MaskE	Single	SNGP	OC	VarProp	ZigZag	
MAE	4.655	4.472	4.699	4.786	4.724	4.819	4.724	4.682	4.630	UTKFACE
rAUC	0.034	0.047	0.043	0.033	0.026	0.031	0.025	0.029	0.045	
Size	1x	5x	1x	1x	1x	1x	1x	1x	1x	
Inf. Time	5x	5x	5x	5x	1x	1x	1x	1x	2x	
Time	1.1x	5x	1.3x	1.2x	1x	1.7x	1.1x	1x	1x	
ROC-AUC	0.688	0.755	0.732	0.653	0.564	0.694	0.658	0.662	0.772	
PR-AUC	0.884	0.939	0.846	0.830	0.762	0.890	0.843	0.851	0.959	
MAE	3.376	3.03	3.03	3.26	3.18	3.16	3.20	3.25	3.10	AIRFOILS
rAUC	0.065	0.062	0.062	0.034	0.008	0.013	0.01	0.015	0.068	
Size	1x	5x	1x	1x	1x	1.05x	1x	1x	1x	
Inf. Time	5x	5x	5x	5x	1x	1.3x	1.1x	1.4x	2x	
Time	1.2x	5x	1.3x	1.3x	1x	1.7x	1.1x	1.1x	1.2x	
ROC-AUC	0.897	0.972	0.971	0.923	0.690	0.894	0.874	0.78	0.992	
PR-AUC	0.744	0.955	0.942	0.793	0.681	0.767	0.748	0.76	0.987	
MAE	0.129	0.101	0.115	0.115	0.121	0.115	0.120	0.119	0.112	CARS
rAUC	0.06	0.10	0.08	0.07	0.03	0.06	0.04	0.03	0.07	
Size	1x	5x	1.05x	1.05x	1x	1x	1x	1x	1x	
Inf. Time	5x	5x	5x	5x	1x	1.3x	1.1x	1.2x	2x	
Time	1.1x	5x	1.2x	1.3x	1x	1.2x	1x	1.1x	1.2x	
ROC-AUC	0.851	0.954	0.921	0.926	0.755	0.872	0.831	0.816	0.956	
PR-AUC	0.734	0.941	0.8669	0.8317	0.534	0.751	0.723	0.567	0.974	
Simple	✓	✓	✗	✗	-	✓	✗	✗	✓	

Table 2. **Regression results on Age Prediction (top), Airfoils (middle) and Cars (bottom).** As in Table 1 the best two results in each category are shown in bold and correspond to *ZigZag* and *DeepE*, except in terms of computation time and memory requirements where *ZigZag* does much better.

overfit the training data. We therefore use the *Deep Layer Aggregation* (DLA) [50] network for our experiments and trained it as recommended in the original paper. We sample our out-of-distribution data from the SVHN dataset that comprises images belonging to classes that are not in CIFAR10, such as road sign digits.

Influence of the Number of Samples. The five-fold increase in computation time that the sampling-based methods incur is a direct consequence of ours using 5 samples. *ZigZag* performs two inferences, which is equivalent to using 2 samples. Thus, in Fig 6, we plot OOD classification performance as a function of the number of samples used.

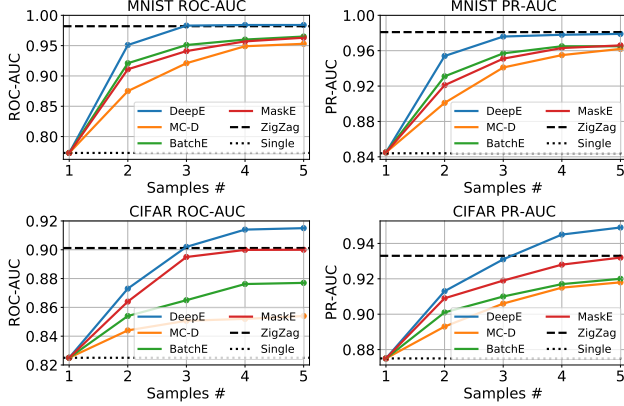


Figure 6. **OOD classification performance as a function of the number of samples.** The dashed line represents the performance of *ZigZag*, which is sampling-free.

When using only 2 or 3 samples, all sampling-based methods perform worse than ours. When using 4 or 5, DeepEnsembles is the only one that performs on par or better than *ZigZag*. However, it then requires at least double the computational budget.

4.4. Regression Tasks.

We report similar results for three very different regression tasks in Tab. 2 that we describe in more detail below. The overall behavior is again similar to what we observed for classification. *ZigZag* performs on par with Deep Ensembles and better than the others, while being much less computationally demanding than Deep Ensembles.

Age Prediction. First, we consider image-based age prediction from face images. To this end, we use UTKFace [51], a large-scale dataset containing tens of thousands of face images annotated with associated age information. We use a network with a large ResNet-152 backbone and five linear layers with ReLU activations. This architecture yield good performance in terms of accuracy, outperforming the popular ordinal regression model CORAL [7] and matching other state-of-the-art approaches such as [4]. As in the classification experiments described above, we use iCartoonFace [52] dataset as out-of-distribution data. It comprises about 400k images of cartoon and anime character faces whose pixel statistics are different from those of the UTKFace while exhibiting a semantic similarity. As before, we train our model on the UTKFace training set and use uncertainty to distinguish UTKFace test set images from iCartoonFace ones.

Predicting Lift-to-Drag Ratios. Our method is generic and can operate with any kind of data. To demonstrate this, we collected a dataset of 2k wing profiles such as those of Fig. 7 by sampling the widely used NACA parameters [20]. We then ran the popular XFOIL simulator [11] to compute

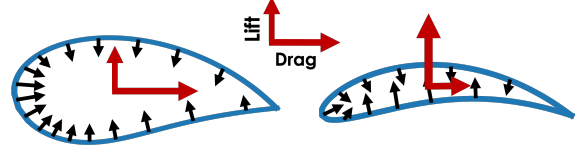


Figure 7. **Airfoil Samples.** Training and testing profiles (left) have reasonable level of aerodynamics, whereas out-of-distribution samples (right) include only top-notch, but rare, shapes in terms of lift-to-drag ratio. The black arrows represent pressures while the red lines depict overall lift and drag.

the pressure distribution along each profile and estimate its lift-to-drag coefficient, a key measure of aerodynamics performance. The resulting dataset consists of wing profiles \mathbf{x}_i represented by a set of 2D nodes and the corresponding scalar lift-to-drag coefficient \mathbf{y}_i for $1 \leq i \leq 2000$.

We took the 5% of top-performing shapes in terms of lift-to-drag ratio to be the out-of-distribution samples. We took 80% of the remaining 95% as our training set and the rest as our test set. Hence, training and testing shapes span lift-to-drag values from 0 to 60, whereas everything beyond that is considered to be OOD and therefore not used for training purposes. We then trained a Graph Neural Network (GNN) that consists of 25 GMM [33] layers with ELU nonlinearities [9] and skip connections [18] to predict lift-to-drag \mathbf{y}_i from profile \mathbf{y}_i for all i in the training set, as in [13, 39]. We provide more details on this network in the supplementary material.

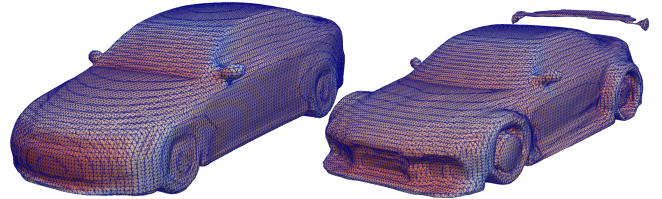


Figure 8. **Cars Models.** The car dataset comprises many regular vehicles (left) with standard aerodynamics and a few streamlined ones (right), which we treat as being out-of-distribution. Red and blue denote high and low pressures respectively.

Predicting the Drag Coefficient of a Car. We performed a similar experiment on 3D car models from a subset of the ShapeNet dataset [8] that features car meshes that are suitable for CFD simulation. We followed the same experimental protocol as for the wings except that we used OpenFOAM [21] to estimate the drag coefficients and a more sophisticated network to predict the drag coefficients from the triangulated 3D meshes representing the cars, which we also describe in the supplementary material.

To consider a more complex and high-dimensional task, we used the same data to train a network to predict not only the drag but also a pressure value at each vertex of a car. To

	Single	MC-D	DeepE	ZigZag
MAE	22.9	20.3	17.9	19.2
rAULC	0.55	0.62	0.68	0.69
ROC-AUC	0.64	0.74	0.83	0.84
PR-AUC	0.63	0.77	0.84	0.82

Table 3. **Pressure Prediction.** Accuracy and calibration are computed for individual predictions for each node of the mesh. AUC metrics are computed using averaged uncertainty of the mesh and the same data splits as for the drag prediction task.

this end, we used the same train-test split as before along with a modified version of the network we used for drag prediction in which we replaced some convolutional layers by transformer layers [40], as explained in the supplementary material. As shown in Fig. 9, *ZigZag* produces per-node uncertainties very similar to those of Deep Ensembles. The most uncertain regions are high curvature parts where pressure changes rapidly. This is reflected by the quantitative results of Tab. 3 that, once again, show *ZigZag* and Deep Ensembles performing similarly.

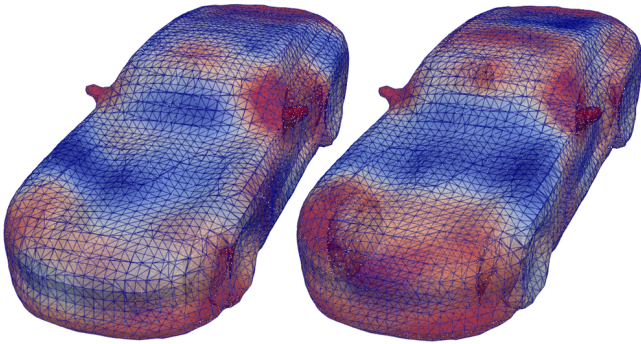


Figure 9. **Pressure Uncertainty for Deep Ensembles (left) and ZigZag (right).** Both approaches produce similar predictions with higher uncertainty in higher curvature areas.

4.5. Analysis

Lipschitz Constants. The theoretical justification of Section 3.2 relies on the networks being Lipschitz. Hence, we estimated the Lipschitz constants $L_{\mathcal{M}}^u$ and $L_{\mathcal{M}}^d$ of the networks we use in Sections 4.2 and 4.4. Since the input spaces are low-dimensional, we sampled them grid-wise and computed ratios of distances between pairs of inputs and the corresponding pairs of outputs. We took the smallest to be the $L_{\mathcal{M}}^u$ estimate we report in Tab. 4 and the largest to be the $L_{\mathcal{M}}^d$ estimate. Plugging these values into Eq. 6 gives us usable error estimation bounds, as shown in the two bottom rows. To confirm that they are meaningful, Fig. 10 shows that the predicted uncertainties and the actual errors are well correlated for the airfoils.

Effective Use of Predictions. Recall from Eq. 3, that we expect our network \mathcal{M} to be trained so that given ground target \mathbf{y} , $\mathbf{y} \approx \mathcal{M}(\mathbf{x}, \mathbf{y})$. To confirm the impor-

	Synth. Class.	Synth. Reg.	Airfoils
$L_{\mathcal{M}}^d$	0.84	0.93	1.27
$L_{\mathcal{M}}^u$	0.61	0.78	0.68
$1/(1 + L_{\mathcal{M}}^d)$	0.54	0.52	0.44
$L_{\mathcal{M}}^u/(1 - L_{\mathcal{M}}^u)$	1.57	3.48	2.13

Table 4. **Empirical Lipschitz Constants** for synthetic classification and regression, as well as for L/D estimation of airfoils. Plugging these numbers into Eq. 6 gives the error bounds below.

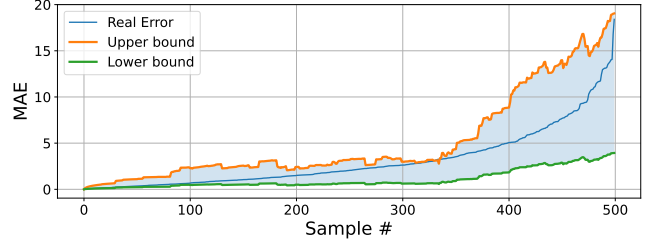


Figure 10. **Estimated uncertainty vs actual error.** We predicted L/Ds and corresponding uncertainties for all 500 test airfoils of Section 4.4. We then ranked them by MAE error, that is, difference between the true L/D and the estimated one shown in blue. Finally, we used Eq. 6 to predict lower and upper bounds for these errors, shown in green and orange. Note that the blue curve is between the other two, as it should.

tance of this, we re-tested *ZigZag* but, instead of feeding to the network its own prediction as input when computing $\mathcal{M}(\mathbf{x}, \mathcal{M}(\mathbf{x}, 0))$, we replaced $\mathcal{M}(\mathbf{x}, 0)$ by the actual ground truth. As shown in Tab. 5, performance significantly increases, which confirms our requirement is fulfilled.

	MNIST	CIFAR
Accuracy	0.982 \rightarrow 1.0	0.93 \rightarrow 0.99
	Airfoils	Cars
MAE	3.10 \rightarrow 0.11	0.112 \rightarrow 0.02

Table 5. **Prediction given ground truth.** Providing the ground-truth as input improves performance, as it should.

5. Conclusion

We have proposed an approach to estimating uncertainty that only requires performing a minor change in the first layer of network to accept an additional argument that may be either blank or the result of that prediction. Training the network to yield the same result in both cases enables us to estimate the uncertainty in a principled way and at low computational cost. This approach is applicable to any practical architecture and requires minimal modifications. It is easy to deploy, generic, and delivers results on par with ensembles at a much reduced training budget. Our error bounds being tightly linked to the Lipschitz properties of our networks, in future work we will explore the feasibility of lowering these constants to boost performance.

References

- [1] Van Amersfoort, J. A. Smith, L. A. Teh, Y. Whye, and Y. Gal. Uncertainty Estimation Using a Single Deep Deterministic Neural Network. In *International Conference on Machine Learning*, pages 9690–9700, 2020. 1, 2
- [2] A. Ashukha, A. Lyzhov, D. Molchanov, and D. Vetrov. Pitfalls of In-Domain Uncertainty Estimation and Ensembling in Deep Learning. In *International Conference on Learning Representations*, 2020. 2
- [3] J. Behrmann, W. Grathwohl, R. Chen, D. Duvenaud, and J. H. Jacobsen. Invertible residual networks. In *International Conference on Machine Learning*, pages 573–582, 2019. 3
- [4] A. Berg, M. Oskarsson, and M. O’Connor. Deep Ordinal Regression with Label Diversity. In *International Conference on Pattern Recognition*, pages 2740–2747, 2021. 7
- [5] Glenn W Brier et al. Verification of Forecasts Expressed in Terms of Probability. *Monthly weather review*, 78(1):1–3, 1950. 4
- [6] Tianle Cai, Shengjie Luo, Keyulu Xu, Di He, Tie-yan Liu, and Liwei Wang. Graphnorm: A principled approach to accelerating graph neural network training. In *International Conference on Machine Learning*, 2021. 12
- [7] W. Cao, V. Mirjalili, and S. Raschka. Rank Consistent Ordinal Regression for Neural Networks with Application to Age Estimation. *Pattern Recognition*, 140:325–331, 2020. 7
- [8] A. Chang, T. Funkhouser, L. G., P. Hanrahan, Q. Huang, Z. Li, S. Savarese, M. Savva, S. Song, H. Su, J. Xiao, L. Yi, and F. Yu. Shapenet: An Information-Rich 3D Model Repository. In *arXiv Preprint*, 2015. 7
- [9] D.-A. Clevert, T. Unterthiner, and S. Hochreiter. Fast and Accurate Deep Network Learning by Exponential Linear Units (ELUs). In *arXiv Preprint*, 2015. 7, 12
- [10] A. Dosovitskiy, L. Beyer, A. Kolesnikov, D. Weissenborn, X. Zhai, T. Unterthiner, M. Dehghani, M. Minderer, G. Heigold, S. Gelly, J. Uszkoreit, and N. Houlsby. An Image is Worth 16x16 Words: Transformers for Image Recognition at Scale. In *arXiv Preprint*, 2020. 3
- [11] M. Drela. XFOIL: An Analysis and Design System for Low Reynolds Number Airfoils. In *Conference on Low Reynolds Number Aerodynamics*, pages 1–12, 1989. 7
- [12] N. Durasov, T. Bagautdinov, P. Baque, and P. Fua. Masksembles for Uncertainty Estimation. In *Conference on Computer Vision and Pattern Recognition*, 2021. 2, 4
- [13] N. Durasov, A. Lukoyanov, J. Donier, and P. Fua. DEBOSH: Deep Bayesian Shape Optimization. In *arXiv Preprint*, 2021. 7
- [14] Marilena Furno and Domenico Vistocco. *Quantile regression: estimation and simulation*, Volume 2, volume 216. John Wiley & Sons, 2018. 2
- [15] Y. Gal. *Uncertainty in Deep Learning*. PhD thesis, University of Cambridge, 2016. 2
- [16] Y. Gal and Z. Ghahramani. Dropout as a Bayesian Approximation: Representing Model Uncertainty in Deep Learning. In *International Conference on Machine Learning*, pages 1050–1059, 2016. 1, 2, 4
- [17] C. Guo, G. Pleiss, Y. Sun, and K. Q. Weinberger. On Calibration of Modern Neural Networks. In *International Conference on Learning Representations*, 2017. 4, 11
- [18] K. He, X. Zhang, S. Ren, and J. Sun. Deep Residual Learning for Image Recognition. In *Conference on Computer Vision and Pattern Recognition*, pages 770–778, 2016. 3, 7, 12
- [19] S. Ioffe and C. Szegedy. Batch Normalization: Accelerating Deep Network Training by Reducing Internal Covariate Shift. In *International Conference on Machine Learning*, 2015. 12
- [20] E Jacobs and Albert Sherman. Airfoil section characteristics as affected by variations of the reynolds number. *Report-National Advisory Committee for Aeronautics*, (577-611):227, 1937. 7
- [21] Hrvoje Jasak, Aleksandar Jemcov, Zeljko Tukovic, et al. OpenFOAM: A C++ Library for Complex Physics Simulations. In *International workshop on coupled methods in numerical dynamics*, 2007. 7
- [22] A. Kendall and Y. Gal. What Uncertainties Do We Need in Bayesian Deep Learning for Computer Vision? In *Advances in Neural Information Processing Systems*, 2017. 4, 12
- [23] D. P. Kingma and J. Ba. Adam: A Method for Stochastic Optimisation. In *International Conference on Learning Representations*, 2015. 12
- [24] Alex Krizhevsky, Vinod Nair, and Geoffrey Hinton. The CIFAR-10 Dataset. *online: http://www.cs.toronto.edu/kriz/cifar.html*, 55(5), 2014. 5
- [25] B. Lakshminarayanan, A. Pritzel, and C. Blundell. Simple and Scalable Predictive Uncertainty Estimation Using Deep Ensembles. In *Advances in Neural Information Processing Systems*, 2017. 1, 2, 4
- [26] Y. LeCun, L. Bottou, Y. Bengio, and P. Haffner. Gradient-Based Learning Applied to Document Recognition. *Proceedings of the IEEE*, pages 2278–2324, 1998. 5
- [27] J. Liu, Z. Lin, S. Padhy, D. Tran, T. B. Weiss, and B. Lakshminarayanan. Simple and Principled Uncertainty Estimation with Deterministic Deep Learning via Distance Awareness. In *Advances in Neural Information Processing Systems*, 2020. 2, 4
- [28] Antonio Loquercio, Mattia Segu, and Davide Scaramuzza. A General Framework for Uncertainty Estimation in Deep Learning. *IEEE Robotics and Automation Letters*, 5(2):3153–3160, 2020. 2
- [29] D. J. Mackay. Bayesian Neural Networks and Density Networks. *Nuclear Instruments and Methods in Physics Research Section A: Accelerators, Spectrometers, Detectors and Associated Equipment*, 354(1):73–80, 1995. 2
- [30] A. Malinin, S. Chervontsev, I. Provilkov, and M. Gales. Regression Prior Networks. In *arXiv Preprint*, 2020. 2
- [31] A. Malinin and M. Gales. Predictive Uncertainty Estimation via Prior Networks. In *Advances in Neural Information Processing Systems*, 2018. 1, 2, 4
- [32] T. Miyato, T. Kataoka, M. Koyama, and Y. Yoshida. Spectral Normalization for Generative Adversarial Networks. In *International Conference on Learning Representations*, 2018. 2, 12

- [33] F. Monti, D. Boscaini, J. Masci, E. Rodolà, J. Svoboda, and M. M. Bronstein. Geometric Deep Learning on Graphs and Manifolds Using Mixture Model CNNs. In *Conference on Computer Vision and Pattern Recognition*, pages 5425–5434, 2017. 7, 12
- [34] J. Mukhoti, van Amersfoort, J. A. Torr, P. HS, and Y. Gal. Deep Deterministic Uncertainty for Semantic Segmentation. In *arXiv Preprint*, 2021. 1
- [35] Y. Netzer, T. Wang, A. Coates, A. Bissacco, B. Wu, and A. Ng. Reading Digits in Natural Images with Unsupervised Feature Learning. In *Advances in Neural Information Processing Systems*, 2011. 5
- [36] J. Postels, F. Ferroni, H. Coskun, N. Navab, and F. Tombari. Sampling-Free Epistemic Uncertainty Estimation Using Approximated Variance Propagation. In *Conference on Computer Vision and Pattern Recognition*, pages 2931–2940, 2019. 1, 2, 4, 12
- [37] J. Postels, M. Segu, T. Sun, L. Van Gool, F. Yu, and F. Tombari. On the Practicality of Deterministic Epistemic Uncertainty. In *arXiv Preprint*, 2021. 2, 4, 5, 11, 12
- [38] A. Rahimi and B. Recht. Random Features for Large-Scale Kernel Machines. In *Advances in Neural Information Processing Systems*, pages 1177–1184, 2007. 2, 12
- [39] E. Remelli, A. Lukoianov, S. Richter, B. Guillard, T. Bagautdinov, P. Baque, and P. Fua. Meshsdf: Differentiable Iso-Surface Extraction. In *Advances in Neural Information Processing Systems*, 2020. 7
- [40] Y. Shi, Z. Huang, S. Feng, H. Zhong, W. Wang, and Y. Sun. Masked Label Prediction: Unified Message Passing Model for Semi-Supervised Classification. In *arXiv Preprint*, 2020. 8, 12
- [41] K. Simonyan, A. Vedaldi, and A. Zisserman. Learning Local Feature Descriptors Using Convex Optimisation. *IEEE Transactions on Pattern Analysis and Machine Intelligence*, 2014. 3
- [42] Lewis Smith, Joost van Amersfoort, Haiwen Huang, Stephen Roberts, and Yarin Gal. Can Convolutional Resnets Approximately Preserve Input Distances? a Frequency Analysis Perspective. In *arXiv Preprint*, 2021. 2, 3
- [43] N. Tagasovska and D. Lopez-Paz. Frequentist Uncertainty Estimates for Deep Learning. In *arXiv Preprint*, 2018. 1, 2
- [44] N. Tagasovska and D. Lopez-Paz. Single-Model Uncertainties for Deep Learning. In *Advances in Neural Information Processing Systems*, 2019. 4
- [45] A. Virmaux and K. Scaman. Lipschitz Regularity of Deep Neural Networks: Analysis and Efficient Estimation. In *Advances in Neural Information Processing Systems*, 2018. 2, 3
- [46] M. Vuk and T. Curk. ROC curve, lift chart and calibration plot. *Advances in methodology and Statistics*, 3(1):89–108, 2006. 11
- [47] A. Weller and T. Jebara. Approximating the Bethe Partition Function. In *Uncertainty in Artificial Intelligence*, 2014. 2
- [48] Y. Wen, D. Tran, and J. Ba. Batchensemble: An Alternative Approach to Efficient Ensemble and Lifelong Learning. In *International Conference on Learning Representations*, 2020. 4
- [49] H. Xiao, K. Rasul, and R. Vollgraf. Fashion-Mnist: A Novel Image Dataset for Benchmarking Machine Learning Algorithms. In *arXiv Preprint*, 2017. 5
- [50] F. Yu, D. Wang, E. Shelhamer, and T. Darrell. Deep Layer Aggregation. In *Conference on Computer Vision and Pattern Recognition*, pages 2403–2412, 2018. 6, 12
- [51] Zhifei Zhang, Yang Song, , and Hairong Qi. Age Progression/regression by Conditional Adversarial Autoencoder. In *Conference on Computer Vision and Pattern Recognition*, 2017. 7
- [52] Y. Zheng, Y. Zhao, M. Ren, H. Yan, X. Lu, J. Liu, and J. Li. Cartoon Face Recognition: A Benchmark Dataset. In *Proceedings of the 28th ACM international conference on multimedia*, pages 2264–2272, 2020. 7

A. Supplementary Material

In this appendix, we give the full derivation for the error bounds of Section 3.2, which we use to justify using the distance $\hat{\mathbf{u}}$ of Eq. 2 to estimate the uncertainty of a model. We then describe the calibration metrics we use and provide additional details about the baselines and training setups used in experimental section.

A.1. ZigZag’s Error Bounds

Eq. 6 shows that our uncertainty estimates are related to the true errors our model makes by quantities that depend on the Lipschitz constants of the networks we use. We now provide the complete proof.

Notation and Definitions. To prove inequalities from Eq. 6, we re-introduce the notation for the three different modes of operation for a trained network \mathcal{M} , as described in Section 3. First, we have regular inference without any information about \mathbf{y} . In this case, the second argument to the network is $\mathbf{0}$ and we write

$$\mathbf{y}_0 = \mathcal{M}(\mathbf{x}, \mathbf{0}) . \quad (9)$$

Then, we can plug this new prediction \mathbf{y}_0 into the network and use it as an input during inference. Now, the new prediction becomes

$$\mathbf{y}_1 = \mathcal{M}(\mathbf{x}, \mathbf{y}_0) = \mathcal{M}(\mathbf{x}, \mathcal{M}(\mathbf{x}, \mathbf{0})) . \quad (10)$$

Finally, a third option is to use the real ground-truth \mathbf{y} as the optional input. The network is trained so that

$$\begin{aligned} \mathbf{y} &\approx \tilde{\mathbf{y}} = \mathcal{M}(\mathbf{x}, \mathbf{y}) , \\ \Rightarrow \delta &= \|\tilde{\mathbf{y}} - \mathbf{y}\| \approx 0 . \end{aligned} \quad (11)$$

Error Lower Bound. First, we derive the left part of Eq. 6. in Section 3.2, that is, the leftmost lower bound of the error

$$\frac{1}{(1 + L_{\mathcal{M}}^d)} \|\mathbf{y}_0 - \mathbf{y}_1\| \leq \|\mathbf{y}_0 - \mathbf{y}\| . \quad (12)$$

Given the definitions of Lipschitz regularity from Section 3, we write

$$\begin{aligned} \|\mathcal{M}(\mathbf{x}, \mathbf{y}) - \mathcal{M}(\mathbf{x}, \mathbf{y}_0)\| &= \|\tilde{\mathbf{y}} - \mathbf{y}_1\| \\ &\leq L_{\mathcal{M}}^d \|\mathbf{x}, \mathbf{y}) - (\mathbf{x}, \mathbf{y}_0)\| = L_{\mathcal{M}}^d \|\mathbf{y} - \mathbf{y}_0\| . \end{aligned} \quad (13)$$

Injecting the triangle inequality of Eq. 3 into Eq. 13 yields

$$\begin{aligned} \|\mathbf{y}_0 - \mathbf{y}_1\| &\leq \|\tilde{\mathbf{y}} - \mathbf{y}_0\| + \|\tilde{\mathbf{y}} - \mathbf{y}_1\| , \\ &\leq \|\tilde{\mathbf{y}} - \mathbf{y}_0\| + L_{\mathcal{M}}^d \|\mathbf{y} - \mathbf{y}_0\| , \\ &\leq \|\tilde{\mathbf{y}} - \mathbf{y}\| + \|\mathbf{y}_0 - \mathbf{y}\| + L_{\mathcal{M}}^d \|\mathbf{y}_0 - \mathbf{y}\| , \\ &\leq \delta + (1 + L_{\mathcal{M}}^d) \|\mathbf{y}_0 - \mathbf{y}\| . \end{aligned} \quad (14)$$

Setting $\delta = 0$ in Eq. 14 yields Eq. 12 and is justifiable because the network is trained so that $\delta \approx 0$.

Error Upper Bound. As mentioned in Section 3.2, deriving the upper bound requires a version bi-Lipschitz regularity from Eq. 5: Given input image \mathbf{x} and optional inputs \mathbf{z}_1 and \mathbf{z}_2 , we require our model to fulfill

$$\begin{aligned} \|(\mathbf{x}, \mathbf{z}_1) - (\mathbf{x}, \mathbf{z}_2)\| &= \|\mathbf{z}_1 - \mathbf{z}_2\| , \\ &\leq L_{\mathcal{M}}^u \|\mathcal{M}(\mathbf{x}, \mathbf{z}_1) - \mathcal{M}(\mathbf{x}, \mathbf{z}_2)\| , \end{aligned} \quad (15)$$

for $L_{\mathcal{M}}^u < 1$. This means that given different optional inputs \mathbf{z}_1 and \mathbf{z}_2 our model generates different predictions. This assumption is natural given the training procedure of Section 3.4 that enforces $(\mathbf{x}, \mathbf{y}) \rightarrow \mathbf{y}$ mapping. Combining Eq. 15 and the triangle inequality Eq. 3 yields

$$\begin{aligned} \|\mathbf{y}_0 - \mathbf{y}\| &\leq L_{\mathcal{M}}^u \|\mathbf{y}_1 - \tilde{\mathbf{y}}\| , \\ &\leq L_{\mathcal{M}}^u (\|\mathbf{y}_1 - \mathbf{y}_0\| + \|\mathbf{y}_0 - \mathbf{y}\| + \delta) , \\ &\leq L_{\mathcal{M}}^u (\|\mathbf{y}_1 - \mathbf{y}_0\| + \delta) + L_{\mathcal{M}}^u \|\mathbf{y}_0 - \mathbf{y}\| , \\ \Rightarrow \|\mathbf{y}_0 - \mathbf{y}\| &\leq \frac{L_{\mathcal{M}}^u}{(1 - L_{\mathcal{M}}^u)} (\|\mathbf{y}_0 - \mathbf{y}_1\| + \delta) . \end{aligned} \quad (16)$$

Setting $\delta = 0$ as before, yields the desired upper bound

$$\|\mathbf{y}_0 - \mathbf{y}\| \leq \frac{L_{\mathcal{M}}^u}{(1 - L_{\mathcal{M}}^u)} \|\mathbf{y}_0 - \mathbf{y}_1\| . \quad (17)$$

A.2. Calibration metrics

In this section, we will describe metrics used for calibration evaluation both for classification and regression tasks. Typical calibration metrics such as *Expected Calibration Error* (ECE) [17] require uncertainties to be express in probabilistic form, which is not the case for many single-shot uncertainty methods. Therefore, unified calibration should be utilized that suits all of the available methods. One of such metrics is *Relative Area Under the Lift Curve* (rAULC) [37] which is based on the *Area Under the Lift Curve* [46].

This metric is obtained by ordering the samples according to increasing uncertainty and calculating the accuracy of all samples with an uncertainty value smaller than a particular quantile. More formally, producing uncertainty value \mathbf{u}_i for every sample in our evaluation set, we also generate an array of uncertainty quantiles $\mathbf{q}_j \in [0, 1], i \in [1, \dots, S]$, with the quantile step equal to $1/S$. Iterating over quantiles \mathbf{q}_j , we compute the performance of our model $F(\mathbf{q}_j)$ using only samples for which uncertainty is less than this quantile. Finally, following notation from [37] we compute AULC metric as

$$AULC = -1 + \sum_S \frac{1}{S} \frac{F(\mathbf{q}_j)}{F_R(\mathbf{q}_j)} ,$$

where $F_R(\mathbf{q}_j)$ represents performance for baseline uncertainty that corresponds to random ordering. Further, in order to compute rAULC we divide AULC with the value of

AULC produced by ideal (optimal) uncertainty model that perfectly orders all of the samples in order of increasing error. Following [37], we use accuracy as $F(\mathbf{q}_j)$ for classification. Similarly, we extend AULC and rAULC to regression tasks via using as $F(\mathbf{q}_j)$ an inverse of *Mean Absolute Error* (MAE) computed for samples with uncertainties less than \mathbf{q}_j .

A.3. Training Details and Baselines

Synthetic Regression For our synthetic regression experiments, we use the architecture that consists of 6 linear blocks, ELU [9] activations, BatchNorms [19] and skip-connections [18]. We train the model for 4000 epochs using Adam [23] optimizer with 10^{-2} learning rate and *mean squared error* loss. For *Single* baseline, we utilize loss from [22] to enable uncertainty estimation. *Deep Ensembles* baseline uses 5 trained single models to extract mean and variance from predictions. For *MC-Dropout*, we apply dropout with 0.2 dropout rate to the last 2 linear layers and sample 5 different predictions during inference. Lastly, for *ZigZag* we extend the first layer of single model to take two inputs and train it the same way as original model.

Synthetic Classification For synthetic classification experiments, we adopt simple feed-forward neural network that comprise of 10 linear layers with ELU activation and skip-connections. As for regression, we apply Adam optimizer for 300 epochs and 10^{-2} learning rate. *Deep Ensembles* also consists of 5 models, *MC-Dropout* drops activations from the last two layers with 0.15 drop rate, *ZigZag* extends the first layer of the original model so it is able to process additional inputs.

MNIST Model used for MNIST experiments consists of two convolutional layers with max pooling followed by three linear layers with LeakyReLU activations. We also train this model using Adam optimizer for three epochs with 10^{-2} learning rate. *MC-Dropout*, *BatchEnsemble* and *Masksembles* are applied to the last two layers of the model with 0.2 drop rate for *MC-Dropout* and 1.5 scale factor for *Masksembles*. *VarProp* propagates variance through the last three linear layers as it was described in [36]. *SNGP* applies Random Features [38] to the last layer of the model and Spectral Normalization [32] to the rest. *OC* extracts features after convolutional layers and train five small models that represent certificates.

CIFAR For CIFAR experiments, we use DLA [50] network and adopt original training setup: network is trained with SGD optimizer with 0.9 momentum for 20 epochs with 10^{-1} learning rate and 10 more epochs with 10^{-2} . As before, *MC-Dropout*, *BatchEnsemble* and *Masksembles* are

applied to the last three layers of the model with 0.1 drop rate and 1.5 scale factor. Features for *OC* are taken after convolutional part of the model.

Age Prediction As an age predictor, we use common Resnet [18] backbone followed by five linear layers with LeakyReLU activations. As before, *MC-Dropout*, *BatchEnsemble* and *Masksembles* are applied to the last four layers of the model with 0.1 drop rate and 1.5 scale factor. *Varprop* propagates variance through the last five layers of the network. *OC* uses features from penultimate layer and trains five small feed-forward networks for certificates.

Airfoils Lift-to-Drag Lift-to-Drag ratio is predicted with custom model that consists of twenty five GMM [33] layers, global max pooling and five linear layers with applied ReLU activations. The model is trained for 10 epochs with Adam optimizer and 10^{-3} learning rate. All of the uncertainty baselines follow the same setup described for age prediction experiments.

Cars Drag In order to predict drag for a car mesh, we utilize similar model to airfoil experiments but with increased capacity. Instead of twenty five GMM layers, we use thirty five and also apply skip-connections with ELU activations. Final model is being trained for 100 epochs with Adam optimizer and 10^{-3} learning rate. All of the uncertainty methods are applied to non-graphical part of the model – last five linear layers. As before, *MC-Dropout* uses 0.05 drop rate, *Masksembles* use 1.5 scale factor, *SNGP* applies Spectral Normalization to the last five layers and *OC* extract features right after max pooling layer.

For pressure prediction task, we modified original architecture and replaced GMM layers with Transformer layers [40] for more fine-grained predictions. In addition, we use GraphNorm [6] after each convolution for faster training and increase total size of the model to seventy layers. The model is being trained for 1500 epochs with Adam optimizer with 10^{-3} learning rate. Implemented uncertainty baselines are replicated from drag prediction experiments.